J Solid State Electrochem (2008) 12:1159–1166
DOI 10.1007/s10008-007-0466-2

ORIGINAL PAPER

Electrochemical study of methylene blue/titanate nanotubes nanocomposite and its layer-by-layer assembly multilayer films

MingWei Xiao · LiShi Wang · YanDan Wu · XinJian Huang · Zhi Dang

Received: 21 August 2007 / Revised: 19 October 2007 / Accepted: 29 October 2007 / Published online: 23 November 2007

Abstract Titanate nanotubes (TNT) were proven to be efficient support for the immobilization of methylene blue (MB). UV–vis absorption and Fourier transform infrared spectra showed that the effect of MB absorbed on TNT was better than nanocrystalline anatase TiO_2 (TNP). The quantity of MB absorbed onto TNT was found to be greater than that of TNP and the electrode modified with the MB–TNT film was more stable due to the strong interaction between TNT and MB as well. The absorption of MB on TNT was impacted by the pH value of the reaction solution for the change of surface charge. Electrochemical oxidation of dopamine (DA) at different electrodes was studied. The result showed that the MB–TNT composite film exhibited excellent catalytic activities to DA compared to those of pure TNT, which is a result of the great promotion of the electron-transfer rate between DA and the electrode surface by the MB–TNT film. Furthermore, the layer-by-layer self-assembly behavior of the electrochemically functional MB–TNT nanocomposite was also discussed after obtaining the stable colloid suspension of MB–TNT. The excellent electrochemical ability and the easy fabrication of layered nanocomposite make the MB–TNT nanocomposite very promising in electrochemistry study and new nanotube-based devices.

Keywords Titanate nanotubes · Methylene blue · Layer by layer · Electrochemically functional nanocomposite

M. Xiao · Y. Wu · Z. Dang
College of Environmental Science and Engineering,
South China University of Technology,
Guangzhou 510640, People's Republic of China

L. Wang (✉) · X. Huang
College of Chemical Science,
South China University of Technology,
Guangzhou 510640, People's Republic of China
e-mail: wanglsh@scut.edu.cn

Introduction

Recently, a lot of attention has been paid to one-dimensional (1-D) TiO_2 nanostructures such as nanotubes, nanowires, nanofibers, and nanoribbons [1–4]. Among 1-D TiO_2 nanostructures, titanate nanotubes (TNT) have become one of the most powerful and promising material in various fields [5]. In fact, their unique physicochemical properties and unusual morphology render TNT very suitable for many applications, such as catalysis [6], electrocatalysis [7–9], and photocatalysis [10–12]. Many researches have been done to study the synthesis process and the structure of these nanotubes, and great development was achieved [13–16]. Increasing interests are being focused on many possible applications of TNT as the substrate decorated with different active catalyst over the last few years [17–20]. TNT composed of corrugated ribbons of edge-sharing TiO_6 octahedra are multilayered structures with a nanometer-scale inner-core cavity exposed to the outer surface and are easily negatively charged because of the protonic nature of its $H_2Ti_3O_7$ structure [21]. These interesting properties of TNT make it an ideal substrate and carrier of active catalyst that need to be immobilized. Furthermore, attempts to date have witnessed successes in the loading of enzymes, metal nanoparticles, and metal ion. Most of the loading improve redox reactions because of the semiconducting properties of the strong

electronic interaction between the support and catalyst for TNT [22–25]. All these interesting properties of TNT encourage us to investigate it as a support for different catalysts.

Methylene blue (MB), a cationic dye whose electrochemical properties are well known in the solution phase, has been used as a redox indicator because its formal potential is between 0.08 and −0.25 V (vs saturated calomel electrode (SCE)) in solution with pH 2–8 [26]. Because the molecular weight of MB is low and the interaction between MB and bare electrode is relativity weak, it can be interpreted by the leakage of MB molecules on the electrode surface and the loss in the mass of absorbed MB molecule. To explore methods to increase the mass absorbed on the electrode surface and improve the stability of the modified electrode, great efforts have been devoted to the characterization of the electrochemistry of MB using electrodes modified with nanomaterials such as nano-Cu_2O [27], carbon nanotubes [28], and nano-SiO_2 [29].

Nanotubular titanium dioxide, the new type of catalysis material possessing a unique combination of physicochemical properties, is a kind of ideal support for different materials through high cation exchange and strong interaction of ion. Moreover, high specific surface area can make more material absorb and the performance better. MB, which is positive in neutral media, is expected to strongly interact with the TNT to form a new kind of stable MB–TNT nanostructure. More importantly, MB possesses good electrochemical properties and the MB^+/MB redox couple has a high self-exchange rate to facilitate the charge transport, which has been widely used for electrocatalysis of biomolecule [30–32]. Therefore, the special properties of the two materials may make the MB–TNT nanocomposite become a promising nanostructure in future applications such as photocatalysis, photovoltaic cells, and electrochemistry. Herein, we reported an alternative strategy to use TNT as efficient support to immobilize MB. For comparison, TiO_2 anatase nanoparticles (TNP) decorated with MB was also used. As demonstrated in the text, the quantity of MB absorbed onto TNT was found to be greater than that of TNP and the electrode modified with the MB–TNT film was more stable than other electrodes as well. In addition, the study of dopamine (DA) electrocatalysis on MB–TNT nanocomposite film and the layer-by-layer assembling multilayer films of the prepared electrochemically functional nanostructure after obtaining a stable colloid suspension were also reported. To the best of our knowledge, the present strategy for the preparation of an electrochemically functional nanocomposite through the adsorption of electroactive MB onto the TNT and the layer-by-layer method has not been reported so far. The prepared MB–TNT nanocomposite is believed to be useful for electrochemical and photovoltaic cells studies.

Experimental

Reagents

TiO_2 (produced by Shanghai Haiyi Scientific & Trading), poly (diallyldimethylammonium chloride) (PDDA; M_w= 20,000), sodium poly (styrenesulfonate) (PSS; M_w= 70,000), and tetraethylammonium hydroxide (TEAOH) were purchased from Aldrich and used as received. DA was purchased from Fluka. MB and other chemicals were all obtained from the chemical reagents company of Guangzhou (China). All other reagents were of analytical reagent grade and used without further purification. Doubly distilled water was used in all aqueous solution preparations and washings.

Titanate nanotubes synthesis

TNT were prepared following a literature procedure [33]. Briefly, 2 g of titanium dioxide (anatase) was added to 50 ml of 10 M NaOH solution and heated for 24 h at 130 °C in a Teflon-lined autoclave. After cooling naturally in air, the mixtures were centrifuged at a speed of 4,000 rpm and the precipitates were collected. The white, powdery sample was thoroughly washed with water then with 0.1 M HCl, followed by vacuum drying at 80 °C.

Preparation of MB–TNT and MB–TNP

The MB–TNT adsorptive nanostructure was prepared by sonicating a mixture consisting of 20 mg of TNT and 10 mg of MB in 10 ml of distilled water for 2 h at room temperature. The resulting suspension was separated by 4,000 rpm centrifugation. The obtained sample was first thoroughly rinsed with distilled water to remove nonadsorbed MB and then dried at 80 °C for 4 h to obtain the MB–TNT nanocomposite. The MB–TNP was prepared by using a suitable amount of anatase TiO_2 nanoparticles in a similar way.

Fabrication of MB–TNT and MB–TNP modified electrode

The glassy carbon electrodes (GCE) were first polished with emery paper (# 2000), 0.3 and 0.05 μm alumina slurry on a woolen cloth, then cleaned under bath sonication for 10 min, and finally thoroughly rinsed with distilled water. The suspension solution of TNT was prepared as follows: 20 mg aliquot of the MB–TNT powder was dispersed in 20 ml of 0.1 M HNO_3 solution to replace the sodium ions with protons by stirring for 30 min. The deposit was separated by centrifuging at 4,000 rpm for 5 min and was then subsequently dispersed in 5 ml of 0.1 M TEAOH under stirring for 5 h at room temperature, which resulted in

a translucent suspension [34]. This suspension was further diluted to 1 mg/ml and the pH was adjusted to neutral by using 0.1 M HCl before use. The TNT-modified electrode (TNT/GCE) was prepared by coating 10 μl of TNT colloidal suspensions onto GCE. The MB–TNT-modified electrode (MB–TNT/GCE) could also be prepared by immersing the TNT/GCE into phosphate buffer (pH 7.0) containing 5.0×10^{-4} M MB for 2 h. The as-prepared MB–TNT/GCE was thoroughly rinsed with water to remove the nonadsorbed MB. For comparison, MB–TNP-modified electrode (MB–TNP/GCE) and MB-modified electrode (MB/GCE) were prepared with the same procedure as that of MB–TNT/GCE. The MB–TNT/GCE at different pH values was prepared by adjusting the pH value of the MB aqueous solution in which the TNT/GCE was immersed.

Fabrication of self-assembled films

A colloidal suspension of MB–TNT nanocomposite was prepared in the same way as that of the TNT colloidal suspension mentioned above. The zeta potential experiment indicated that the pH at the point of zero charge of the MB–TNT nanocomposite was about 8.5. Tin-doped indium oxide on glass (ITO) was used as substrate for multilayer film buildup and was cleaned by sonicating sequentially for 20 min each in acetone, 10% KOH in ethanol, and distilled water. After the treatment, ITO electrodes were rich in negative charges. The cleaned pieces were kept in absolute methanol in plastic containers and were rinsed with water just before use [35, 36]. The procedure for preparing multilayer films was as follows: ITO electrodes with original negative surface charges were treated with aqueous solution of PDDA for 20 min to form positive surfaces before layer-by-layer assembly. Multilayer films were grown by alternately dipping the modified ITO substrates into negatively charged PSS aqueous solution (10 mg/ml) and positively charged complex of MB–TNT aqueous solution (1 mg/ml) for 20 min, respectively. The films were carefully washed with water after each dipping step and then dried with N_2 gas. This sequence was repeated to obtain the desired numbers of layers designated as $\{PSS/MB–TNT\}_n$.

Apparatus

X-ray photoelectron spectroscopy (XPS) measurements were done with AXis Ultra^{DLD} (Kratos). Both transmission electron microscopy (TEM) and scanning electron microscopy measurements were conducted using a JEM-2010HR (JEOL) and a DS-720 (Topcon), respectively. The UV–vis absorption spectra were checked by using a UV3100 spectrophotometer (Shimadzu, Kyoto, Japan). Fourier transform infrared (FT-IR) spectra were recorded with an FT-IR spectrophotometer (Bruker, Germany). The zeta potential was measured by a Zetasizer Nano ZS (Malvern Instruments, UK).

Electrochemical measurements

Measurements were carried out with a computer-controlled CHI660B electrochemical workstation (CHI, Austin, TX, USA) in a conventional three-electrode system using a modified GCE as working electrode, a platinum wire as counter electrode, and a SCE as reference electrode. All potentials were reported in this context with respect to this reference. The electrochemical solution was bubbled with pure nitrogen for 30 min to remove oxygen before measurement. All measurements were performed at room temperature (25 °C).

Results and discussion

Morphological characterization of the prepared TNT

The typical morphologies of the as-prepared TNT were displayed in Fig. 1. The TEM images showed that the TNT present a uniform distribution in an average diameter of

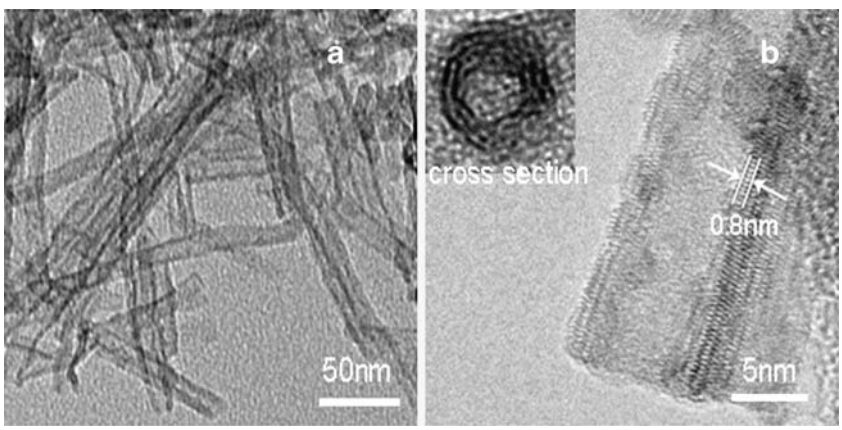

Fig. 1 **a** TEM image of samples; **b** as-prepared TNT, *inset* shows the cross-section

10 nm with the layered structure and the hollow nature of the tubes are always open on both ends, enabling solution filling or nanocluster encapsulation into their tubular cavity (Fig. 1a). A single nanotube was composed of multilayered walls and 5–6-nm inner diameter with an intershell spacing of about 0.8 nm (Fig. 1b).

XPS analysis of MB–TNT nanocomposite

The chemical composition of the TNT and MB–TNT nanocomposite was determined by XPS. The survey spectra were presented in Fig. 2. It can be seen from Fig. 2 that the peaks mainly contain the Ti 2*p* (458.5 eV), O 1*s* (530.7 eV), and C 1*s* (285.4 eV). The peaks of the N 1*s* (399.6 eV) and S 2*p* (164.5 eV) appear in the survey spectra of the MB–TNT nanocomposite. This XPS spectra can serve as an evidence for the formation of the MB–TNT nanocomposite and indicate that the nanocomposite contain not only Ti and O elements but also a small amount of N and S elements, which was the component of MB molecules.

Spectroscopic studies on MB adsorption onto TNT and TNP

The MB–TNT and MB–TNP nanocomposites were studied with UV–vis spectroscopy as shown in Fig. 3. The spectrum of free MB in aqueous solution displayed a strong absorbance at 663 nm, which ascribed to the characteristic of the MB in solution. The absorption of MB onto the TNT was evident from the spectrum of the MB–TNT nanocomposite, which was similar to that of free MB. Compared with that of MB–TNT, the UV–vis spectrum of MB–TNP was not obvious at the absorbance peak of free MB. The absorbance peak for MB–TNT was located at 657 nm, just 6 nm blue shift compared with the free MB aqueous solution. However, the absorbance peak of MB shifted to 592 nm after its adsorption onto the TNP. In contrast with MB–TNP, the UV–vis spectroscopy suggested that there was no obvious characteristic change for MB in MB–TNT. Figure 4 shows the FT-IR spectra of free MB and the MB–TNT and MB–TNP nanostructures. The FT-IR spectrum of free MB exhibited its ring stretch at 1,599 cm^{-1}, the symmetric stretch of C–N at 1,395 cm^{-1}, and the symmetric deformation of $–CH_3$ at 1,339 cm^{-1} [28]. The adsorption of MB onto the TNT was substantial, based on the FT-IR spectra, because the characteristic spectrum of MB was almost uniform in the spectrum of the adsorptive adduct. Moreover, the FT-IR spectrum of free MB was almost consistent with its adsorption onto TNT. For instance, the ring stretching band at 1,599 cm^{-1} was only shifted to 1,600 cm^{-1} and the symmetric deformation

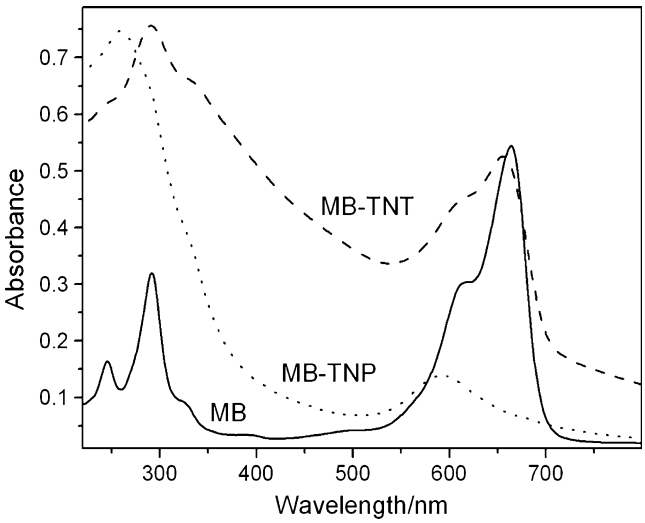

Fig. 3 UV–vis absorbance spectra of MB (*solid curve*) 0.025 g/dm^3 in water, MB–TNT (*dash curve*) 0.1 g/dm^3 in water, and MB–TNP (*dot curve*) 0.1 g/dm^3 in water

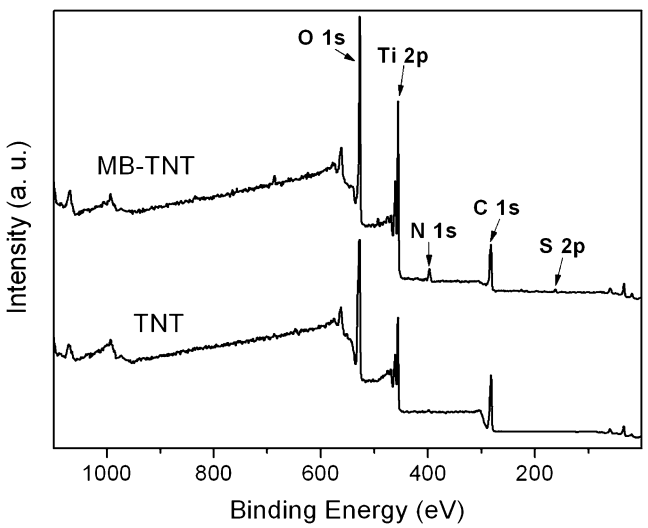

Fig. 2 XPS spectra of TNT and MB–TNT nanocomposite

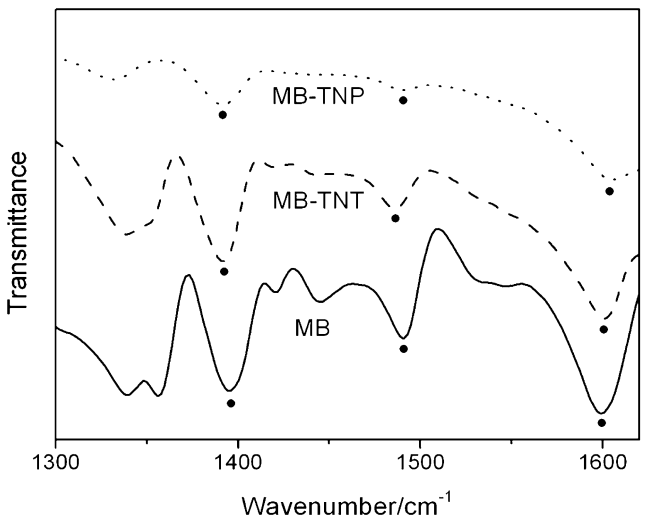

Fig. 4 FT-IR spectra of MB (*solid curve*), MB–TNT (*dash curve*), and MB–TNP (*dot curve*)

of $-CH_3$ at 1,339 cm^{-1} to 1,338 cm^{-1}. Compared with MB–TNT, the FT-IR spectra of MB–TNP showed the worst accordance with MB and the characteristic spectrum of MB in TNP was shifted more than that of MB–TNT. For instance, the ring stretching band and symmetric deformation of $-CH_3$ in TNP were shifted to 1,605 and 1,331 cm^{-1}, respectively. The above spectroscopic studies on MB adsorption onto TNT and TNP strongly showed that the effect of MB absorbed on TNT was better than that of on TNP and more MB molecules deposited onto TNT approximately.

Electrochemical studies of MB–TNT and MB–TNP films

MB, one of the polynuclear aromatic complexes, is a cation in the oxidized state and readily adsorbs onto negatively charged surfaces. Electrochemical studies show that, in aqueous media, MB undergoes a two-electron reduction and shows a stable and reversible signal at a pH-dependent potential [37]. Titanate ($H_2Ti_3O_7$) was a protonic acid, and nanotubes are in a colloidal state with the negatively charged surface after treatment with a weak organic base [38]. MB dissolved in water and readily adsorbed onto negatively charged titanate nanotube surfaces but it was relatively difficult to accumulate onto positively charged TiO_2 nanoparticles in the same condition. Figure 5 compared the typical cyclic voltammograms (CVs; the 1st, 30th, and 60th cycle) obtained at the MB–TNT/GCE (a), MB–TNP/GCE (b), and MB/GCE (c). Figure 5d compared the CVs of different electrodes after 30 cycles as well. From Fig. 5d, we can see that the peak current of MB–TNT was the highest among the electrodes, and the value was nearly three times greater than that of MB–TNP electrode after 30 cycles. It proved that TNT carried a stronger negative surface charge and combined with positive MB molecules tightly and largely through the Coulomb force. On the contrary, the MB–TNP electrode showed that there was less electroactive MB molecules absorbed on TNP/GCE although the peak current was greater than MB/GCE because the absorbance capacity of TNP was smaller. However, we did find that the CV response obtained with the three electrodes decreased gradually upon the first 30th potential cycling and then reached stable value in the next continuous cycle. For MB–TNT/GCE, the peak current reduced by 10% after 30 cycles and became stable in later cycles according to Fig. 5a. In contrast, the decrease of peak current on the MB–TNP/GCE and bare GCE was 27% and 40% according to Fig. 5b and c, respectively, despite that they were also stable after 60 cycles. For MB–TNT, TNT possessed stronger negative charge surface and larger surface area. Consequently, a lot of positive MB molecules combined with TNT closely through the Coulomb force and deposited on the TNT surface. Though some leakage of MB appeared on MB–TNT/GCE, most of the MB molecules remained closely linked to TNT because of the intense Coulomb force

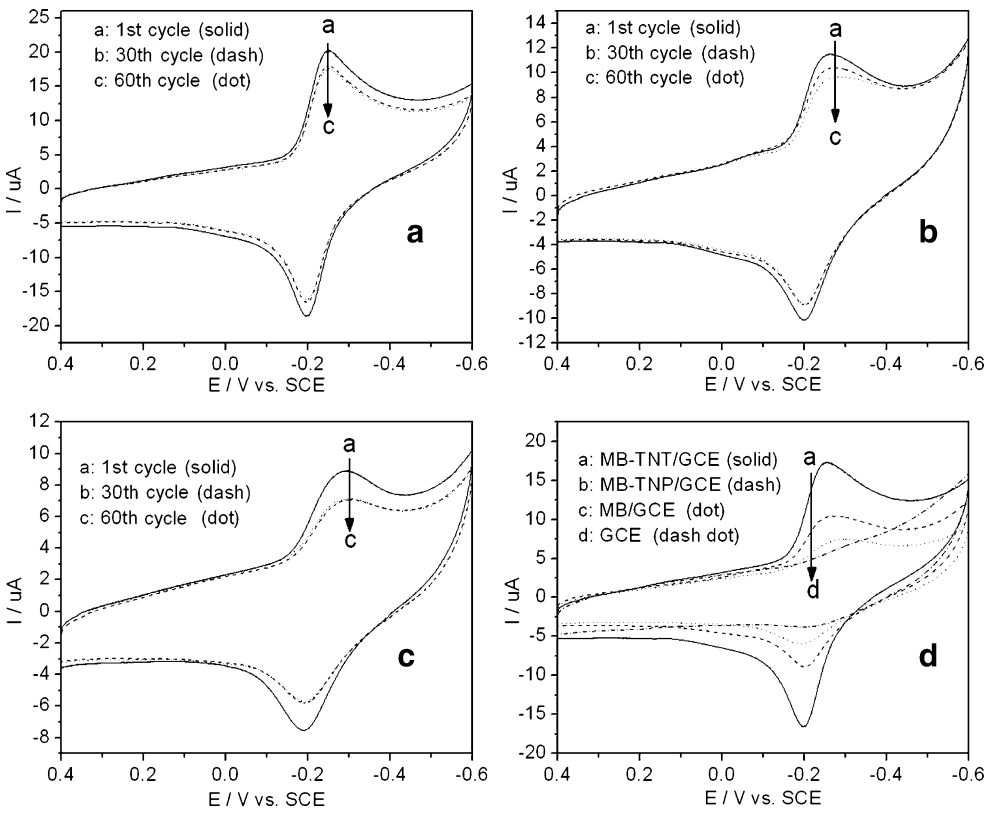

Fig. 5 CVs of MB–TNT/GCE (**a**), MB–TNP/GCE (**b**), and MB/GCE (**c**) in phosphate buffer. *Solid*, *dash*, and *dot curves* represent the 1st, 30th, and 60th cycles, respectively. Scan rate=100 mV/s. (**d**) CVs of different electrodes in the 30th cycle in phosphate buffer. Scan rate=100 mV/s

between the negative TNT and positive MB molecules. From the CVs of MB–TNP/GCE, we can find that the quantity of MB absorption was less and the decrease of peak current was more than that of TNT. TNP, which was of positive charge in neutral media, lacks strong attraction force and has less surface area in contrast to TNT [37]. So, it is reasonable that the positively charged dye show higher affinity for the anionic TNT surface. Similarly, the quantity and stability of MB/GCE was also worse than that of MB–TNT/CCE and MB–TNP/GCE because of the poor adsorption between MB molecules and glassy carbon surface.

From Fig. 5d, a well-defined, nearly reversible redox couple with the apparent formal peak midpoint potential (E_p) of −0.228 V and the peak separation (ΔE_p) of 55 mV was observed for the MB–TNT composite covered with GCE after 30 cycles. The value of anodic peak current (ipa)/cathodic peak current (ipc) was 1.01, which was very close to the value of unity expected when there are no kinetic or other complications in the electrode process. The MB–TNP/GCE showed a quasireversible wave with an E_p of −0.241 V and the ratio of ipa/ipc decreased to 0.88 after 60 cycles. Figure 6 depicted the cyclic voltammograms of the MB–TNT/GCE in phosphate buffer at various scan rates. As shown, the ipa and the ipc increased linearly with the scan rate from 50 to 500 mV/s (inset), which was characteristic of thin-layer electrochemistry, while the potential did not change appreciably. This demonstrated that the redox process of the MB–TNT nanostructure onto the GCE was a fast and surface-confined process.

The pH value is also a very important factor for the formation of MB–TNT nanocomposite because of the changes in surface charge [39–41]. Figure 7 showed the CVs of the MB–TNT/GCE prepared in MB aqueous solution at different pH values. As can be seen in Fig. 7, the peak current of the MB–TNT nanocomposite increased significantly when the pH of the dye solution was changed from 3.0 to 7.0. This result attribute to the change of zeta potential of TNT at different pH values. The pH at the point of zero charge of TNT was about 5.6 according to the zeta potential experiment. At the pH values below 5.6, the cationic MB molecules are relatively difficult to combine with the positive surface of TNT because of electrostatic repulsion. On the contrary, the surface is most negatively charged and cationic MB binds most strongly to the TNT surface when the pH value is higher than 5.6. However, we also found that the peak current increase from pH 7.0 to 9.0 decreased considerably compared with that of from pH 5.0 to 7.0. This might be due to the saturation for MB molecules on the surface of TNT when more MB molecules adsorbed on the TNT with the increase of pH value.

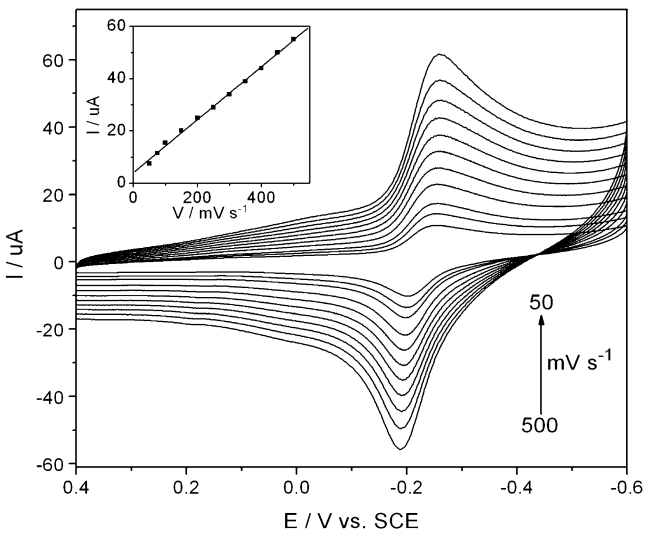

Fig. 6 CVs obtained at the MB–TNT/GCE in phosphate buffer. Scan rate (from inner to outer)=50, 75, 100, 150, 200, 250, 300, 350, 400, 450, and 500 mV/s. *Inset* shows plots of anodic peak currents vs potential scan rate

Electrochemical oxidation of dopamine at MB–TNT/GCE

DA is a compound of great biochemical and neurochemical interest, playing a potential role in human metabolism [42]. CVs of 80 μM DA recorded individually at MB–TNT/GCE (a), TNT/GCE (b), and bare GCE (c) were shown in Fig. 8. DA showed a pair of weak irreversible peaks that appeared at 0.036 and 0.441 V (curve c), possibly due to the fouling of oxidation product on the electrode surface. At TNT/GCE, a pair of peaks appeared at 0.3 and 0.072 V with the peak currents increasing and peak separation decreasing (curve b). This result can be attributed to the diffusion of positively charged DA into negatively charged TNT film. DA is positively charged in neutral media solution [43], and the negative TNT membrane can favor more cationic DA molecules to approach the electrode surface and enhances their electrochemical reaction at the TNT/GCE [44].

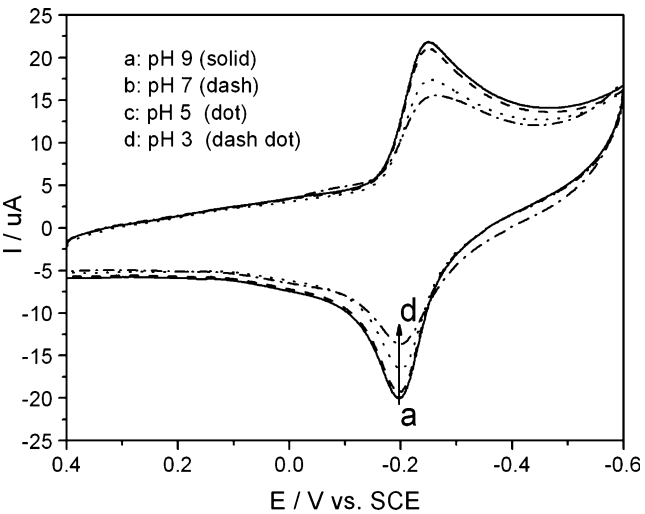

Fig. 7 CVs obtained at the MB–TNT/GCE prepared at pH 9 (a), pH 7 (b), pH 5 (c), and pH 3 (d) in phosphate buffer. Scan rate=100 mV/s

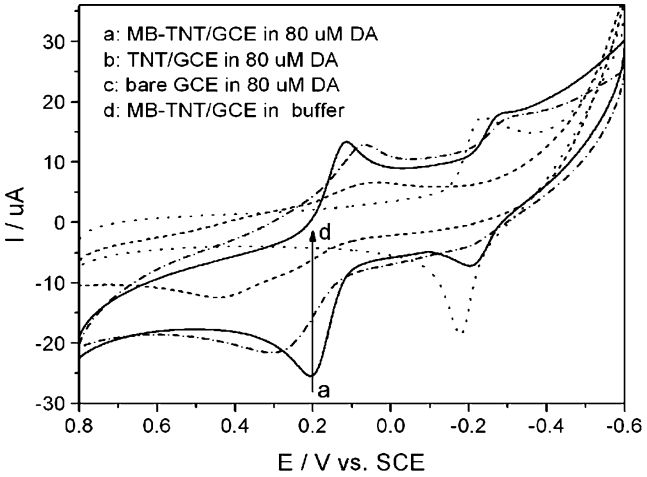

Fig. 8 CVs of MB–TNT/GCE (a), TNT/GCE (b), and bare GCE (c) in the presence of 80 μM DA; MB–TNT/GCE in phosphate buffer (d). Scan rate=100 mV/s

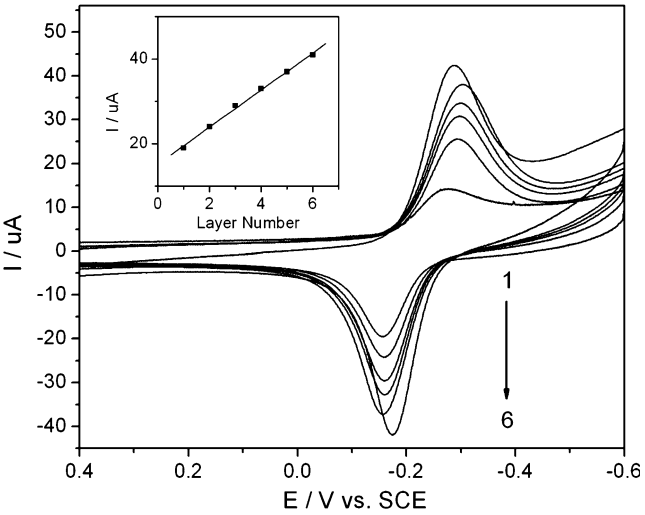

Fig. 9 CVs corresponding to the $\{PSS/MB–TNT\}_n$ multilayer films assembled at ITO electrode in phosphate buffer (pH 7.0) with n=1, 2, 3, …6. *Inset* shows plots of anodic peak currents vs different layer numbers. Scan rate=100 mV/s

However, as can be seen from curve a, at the MB–TNT/GCE, a pair of symmetrical peaks appeared at 0.206 and 0.115 V, with the peak currents increasing dramatically and the oxidation peak potential decreasing to about 200 mV compared to that of bare GCE. According to the result, it is obvious that the MB–TNT nanocomposite achieved higher reversibility and better electrocatalysis effect in the electrochemical oxidation of DA than TNT film. The better electrocatalysis effect of DA at MB–TNT/GCE can be attributed to two reasons. On one hand, the unusual nanotubular structure and the interesting physicochemical properties make TNT more effective in DA electrocatalysis through strong absorption of DA. On the other hand, MB, which possess favorable electron transfer properties [27], serve as an effective electron transfer promoter and improve the electron-transfer rate between DA and electrode surface in the hollow tube of TNT. These factors act together to facilitate DA electrochemical oxidation at the MB–TNT-composite-modified electrode surface.

Characterization of the multilayer film

Cyclic voltammograms could be used as a characterization method for layer-by-layer assembly of electroactive species [45]. Figure 9 showed typical cyclic voltammograms obtained on the $\{MB–TNT/PSS\}_n$-modified ITO electrode in 0.1 M phosphate buffer (pH 7.0) at a scan rate of 0.1 mV/s. The redox peaks currents, which were attributed to the MB molecules, increased with the increase of the assembly cycles and were linear with the layer number (inset; with cathodic peak current) as well. It suggested that the electrochemical property of MB was not changed in the MB–TNT complex and the film of MB–TNT nanocomposite increased uniformly at the ITO electrode. All these were indicative of layer-by-layer assembling of the nanostructure and the same amount of MB–TNT assembled in each layer.

The growth of multilayer film was also monitored by UV–vis spectroscopy. Figure 10 showed the absorbance of the self-assembled $\{PSS/MB–TNT\}_n$ multilayers on the quartz slide. Clearly, there was an absorption peak at about 263 and 600 nm in each bilayer. The former absorbance peak was ascribed to TNT [46] and the latter one was the characteristic peak for MB. The absorbance increased linearly with the growth of layer number (inset in Fig. 10), which indicated that the growth of the film assembly was uniform spectroscopically. When the negatively charged PSS was replaced by positively charged PDDA, no growth of the film was observed. All these

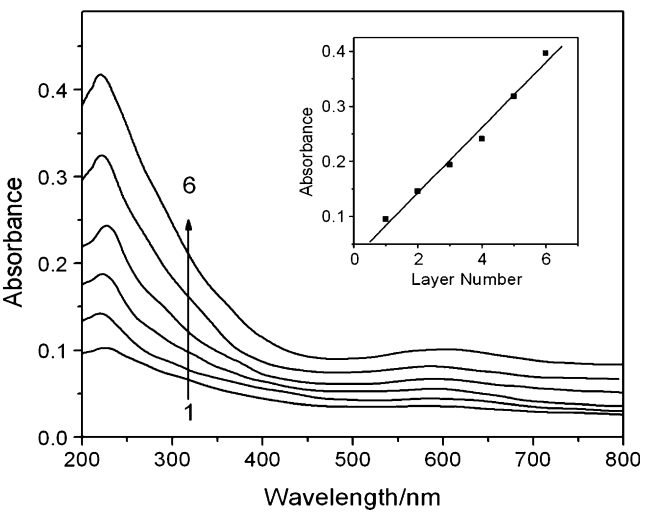

Fig. 10 UV–vis absorption spectra for PSS/MB–TNT multilayer film fabricated from nanotube concentration of 1 g/dm^3 and deposition time of 20 min. *Inset* shows the plot of absorbance at 230 nm vs the number of layer pairs

results further demonstrated the formation of the complex and charge conversion of the MB–TNT nanocomposite.

Conclusions

A comparative study between the immobilization of MB with titanate nanotubes and TiO_2 anatase nanoparticles as the support substrate was carried out. UV–vis absorption and FT-IR spectra showed that the effect of MB absorbed on TNT was better than that of TNP. The electrochemical properties of MB–TNT were studied by cyclic voltammetry and the results demonstrated that the stability of MB–TNT/GCE was the best among the three different electrodes and the redox of MB–TNT at the electrode surface was a surface-controlled process. The pH value of the reaction solution was found to be an important factor for the adsorption of the cationic MB molecule. The electrocatalytical ability of different modified electrodes towards DA was compared and the electrocatalytic mechanism has been discussed. It was found that the MB–TNT-modified electrode showed favorable electrocatalysis to DA. Furthermore, the thin film of the functional nanocomposite was fabricated by an alternate-layer deposition process from a stable, colloidal solution of MB–TNT. An expected electrochemical function of the MB–TNT nanocomposite has been achieved successfully. The excellent electrochemical ability and the easy fabrication of the layered nanocomposite make them very promising materials in electrochemistry study and new nanotube-based devices.

Acknowledgements The financial support from the National Natural Science Foundation of China (No. 20475018) and the Natural Science Foundation of Guangdong (No. 07006544) are gratefully acknowledged.

References

1. Tsai CC, Teng HS (2006) Chem Mater 15:367
2. Yu JG, Yu HG, Cheng B, Zhao XJ, Zhang QJ (2006) J Photochem Photobiol A Chem 182:121
3. Armstrong AR, Armstrong G, Canales J, Bruce PG (2004) Angew Chem Int Ed 43:2286
4. Yu HG, Yu JG, Cheng B, Zhou MH (2006) J Solid State Chem 179:349
5. Bavykin DV, Friedrich JM, Walsh FC (2006) Adv Mater 18:2807
6. Lin CH, Chien SH, Chao JH, Sheu CY, Cheng YC, Huang YJ, Tsai CH (2002) Catal Letters 80:153
7. Qu JP, Zhang XG, Wang YG, Xie CX (2005) Electrochim Acta 50:3576
8. Li JR, Tang ZL, Zhang ZT (2005) Electrochem Commun 7:62
9. Ponce-de-Leon C, Bavykin DV, Walsh FC (2006) Electrochim Acta 8:1655
10. Li H, Zhu BL, Feng YF, Wang SR, Zhang SM, Huang WP (2007) J Solid State Chem 180:2136
11. Yu JG, Yu HG, Cheng B, Trapalis C (2006) J Mol Catal A Chem 249:135
12. Xu JC, Lu M, Guo XY, Lia HL (2005) J Mol Catal A Chem 226:123
13. Bavykin DV, Parmon VN, Lapkin AA, Walsh FC (2004) J Mater Chem 4:3370
14. Zhang S, Peng LM, Chen Q, Du GH, Dawson G, Zhou WZ (2003) Phys Rev Lett 91:256103
15. Kim GS, Ansari SG, Seo HK, Kim YS, Shin HS (2007) J Appl Phys 101:024314
16. Sun XM, Li YD (2003) Chem Eur J 9:2229
17. Bavykin DV, Lapkin AA, Plucinski PK, Murciano LT, Friedrich JM, Walsh FC (2007) Top Catal 39:151
18. Hodos M, Horváth E, Haspel H, Kukovecz Á, Kónya Z, Kiricsi I (2004) Chem Phys Lett 399:512
19. Wang M, Guo DJ, Li HL (2005) J Solid State Chem 178:1996
20. He KX, Zhang XG, Li J (2006) Electrochim Acta 51:1289
21. Chen Q, Zhou WZ, Du GH, Peng LM (2002) Adv Mater 14:1208
22. Murciano LT, Lapkin AA, Bavykin DV, Walsh FC, Wilson K (2007) J Catal 245:272
23. Idakiev V, Yuan ZY, Tabakova T, Su BL (2005) Appl Catal A Gen 281:149
24. Hou LR, Yuan CZ, Peng Y (2007) J Hazard Mater B139:310
25. Wang YG, Wang ZD, Xia YY (2005) Electrochim Acta 50:5641
26. Yao H, Li N, Xu S, Xu JZ, Zhu JJ, Chen HY (2005) Biosens Bioelectron 21:372
27. Liu CY, Hu JF, Hu JM, Tang HW (2006) Electroanalysis 18:478
28. Yan YM, Zhang MN, Gong KP, Su L, Guo ZX, Mao LQ (2005) Chem Mater 17:457
29. Xian YZ, Liu F, Xian Y, Zhou YY, Jin LT (2006) Electrochim Acta 51:6527
30. Lin XH, Wu P, Chen W, Zhang YF, Xia XH (2007) Talanta 72:468
31. Tan L, Yao SZ, Xie QJ (2007) Talanta 71:827
32. Meric B, Kerman K, Ozkan D, Kara P, Erensoy S, Akarca US, Mascini M, Ozsoz M (2002) Talanta 56:837
33. Kasuga T, Hiramatsu M, Hoson A, Sekino T, Niihara K (1998) Langmuir 14:3160
34. Tokudome H, Miyauchi M (2004) Chem Commun 8:958
35. Xu ZA, Gao N, Dong SJ (2006) Talanta 68:753
36. Sha YF, Qian L, Ma Y, Bai HX, Yang XR (2006) Talanta 70:556
37. Bavykin DV, Milsom EV, Marken F, Kim DH, Marsh DH, Riley DJ, Walsh FC, El-Abiary KH, Lapkin AA (2005) Electrochem Commun 7:1050
38. Liu AH, Wei MD, Honma I, Zhou HS (2005) Anal Chem 77:8068
39. Nelson BP, Candal R, Corn RM, Anderson MA (2000) Langmuir 16:6094
40. Muruganandham M, Swaminathan M (2006) Dyes Pigm 68:133
41. Yu JG, Zhao L, Cheng B (2006) Mater Chem Phys 96:311
42. Martin CR, Kohli P (2003) Nat Rev Drug Discov 2:29
43. Yuan S, Hu SS (2004) Electrochim Acta 49:4287
44. Liu AH, Wei MD, Honma I, Zhou HS (2006) Adv Funct Mater 16:371
45. Milsom EV, Novak J, Green SJ, Zhang XH, Stott SJ, Mortimer RJ, Edler K, Marken F (2006) J Solid State Electrochem 11:1109
46. Ma RZ, Sasaki T, Bando Y (2004) J Am Chem Soc 126:10382